Novel General Finite Element Solver for Gyroelectric Structures

Lian Yuh Tio, Lionel E. Davis, Andrew A. P. Gibson and Bernice M. Dillon

Dept. of Electrical Engineering & Electronics, University of Manchester Institute of Science and Technology (UMIST), P.O. Box 88, Sackville Street, Manchester M60 1QD, U.K.

Abstract — **A novel general finite element solver for gyroelectric structures is presented. The solver is validated and compared with known gyrotropic waveguide solutions. Slab loaded semiconductor waveguides are investigated for nonreciprocity and differential phase shift is calculated. The proposed structures can potentially be exploited as nonreciprocal phase shift and control components for terahertz frequencies.**

I. Introduction

Classical nonreciprocal ferrite components such as isolators and circulators operating above 40GHz exhibit poor performance due to material constraints [1,2]. Also, processing incompatibilities between ferrites and semiconductors prohibit the integration of ferrites into MMICs. To overcome these traditional limitations of ferrites, the gyroelectric materials are explored. By considering the semiconductor as a magneto-plasma the Drude model [3] gives rise to a permittivity tensor. This is the dual of the permeability tensor associated with magnetized ferrites. Yong et al [1,2] have demonstrated for the first time that semiconductor junction circulators are possible, but more powerful theoretical tools and further experimental work are required to explore the application of gyroelectric materials to other types of nonreciprocal device.

The finite element method (FEM) is a proven technique for analysing general waveguiding structures. However, transversely magnetised, gyrotropic loaded, waveguide structures pose particular problems for finite element eigenvalue methods. In order to evaluate the propagation constant as the eigenvalue it is necessary to implement a formulation with at least four field components. The formulation proposed by Angkeaw et al [4] uses 4-transverse-field components and can be applied to any gyrotropic waveguide problem. They claim that the formulation is a novel approach to eliminate spurious modes. In this solution, the bias field and frequency are predefined to evaluate the material tensor entry components before the FEM is used to calculate the modal transverse fields and propagation constants.

The formulation is described for any 3×3 material Hermitian tensors. It has been explicitly applied to gyroelectric structures for the first time. Nonreciprocal gyroelectric geometries are investigated and new devices are proposed. Phase constant and field plots are presented. The solver is validated against known ferrite and semiconductor boundary value problems. The theoretical and FEM results yield good agreement.

II. Finite Element Formulation

Consider a gyrotropic waveguide with an arbitrary cross section in the x-y plane. The waveguide is assumed to be uniform along its longitudinal z-axis and its cross section is subdivided into a finite number of elements according to the finite element method. The permittivity and permeability tensors of the gyrotropic medium are assumed to be Hermitian and are defined in matrix form as

$$[\varepsilon]=\begin{bmatrix}\varepsilon_{xx} & \varepsilon_{xy} & \varepsilon_{xz}\\ \varepsilon_{yx} & \varepsilon_{yy} & \varepsilon_{yz}\\ \varepsilon_{zx} & \varepsilon_{zy} & \varepsilon_{zz}\end{bmatrix}=\begin{bmatrix}\varepsilon_{tt} & \varepsilon_{tz}\\ \varepsilon_{zt} & \varepsilon_{zz}\end{bmatrix} \tag{1}$$

$$[\mu]=\begin{bmatrix}\mu_{xx} & \mu_{xy} & \mu_{xz}\\ \mu_{yx} & \mu_{yy} & \mu_{yz}\\ \mu_{zx} & \mu_{zy} & \mu_{zz}\end{bmatrix}=\begin{bmatrix}\mu_{tt} & \mu_{tz}\\ \mu_{zt} & \mu_{zz}\end{bmatrix} \tag{2}$$

where the subscripts *tt*, *tz*, *zt* and *zz* refer to 2×2, 2×1, 1×2 and 1×1 submatrices, respectively.

From Maxwell's equations, the equations that govern the electromagnetic fields in each element can be decoupled to transverse-direction components and longitudinal-direction components. The transverse direction components satisfy the following equations:

$$\omega\varepsilon_{tt}\cdot\boldsymbol{E}_t+\omega\varepsilon_{tz}\cdot\boldsymbol{E}_z+j\nabla_t\times\boldsymbol{H}_z+\beta z\times\boldsymbol{H}_t=0 \tag{3}$$

$$\omega\mu_{tt}\cdot\boldsymbol{H}_t+\omega\mu_{tz}\cdot\boldsymbol{H}_z-j\nabla_t\times\boldsymbol{E}_z-\beta z\times\boldsymbol{E}_t=0 \tag{4}$$

where E_t and H_t are the transverse components of the electric and magnetic fields, respectively. The longitudinal components, E_z and H_z can be expressed in terms of the transverse electromagnetic field components as

$$\boldsymbol{E}_z=\frac{1}{j\omega\varepsilon_{zz}}\left[\nabla_t\times\boldsymbol{H}_t-j\omega\varepsilon_{zt}\cdot\boldsymbol{E}_t\right] \tag{5}$$

0-7803-7695-1/03/$17.00 © 2003 IEEE

$$H_z = \frac{-1}{j\omega\mu_{zz}}\left[\nabla_t \times E_t + j\omega\mu_{zt} \cdot H_t\right] \quad (6)$$

Substituting (5) and (6) into (3) and (4) will yield equations in terms of transverse field components before they are pre-dot multiplied with test functions, E_t^* and H_t^*, respectively. They are then integrated by parts over the whole domain of consideration before adding them together to obtain a variational functional. By applying the appropriate boundary conditions, the boundary integral terms vanish and the resultant functional is:

$$\begin{aligned}\int_s \Big[& E_t^* \cdot \omega\varepsilon_{tt} \cdot E_t + H_t^* \cdot \omega\mu_{tt} \cdot H_t \\ & - \frac{1}{\omega\mu_{zz}}\left[\nabla_t \times E_t + j\omega\mu_{zt} \cdot H_t\right]^* \cdot \left[\nabla_t \times E_t + j\omega\mu_{zt} \cdot H_t\right] \\ & - \frac{1}{\omega\varepsilon_{zz}}\left[\nabla_t \times H_t - j\omega\varepsilon_{zt} \cdot E_t\right]^* \left[\nabla_t \times H_t - j\omega\varepsilon_{zt} \cdot E_t\right]\Big] ds \\ & = \beta \int_s z \cdot \left[E_t^* \times H_t + E_t \times H_t^*\right] ds\end{aligned} \quad (7)$$

When gyroelectric structures are considered, all the off-diagonal permeability tensor entries will go to zero, leaving scalar values for the diagonal permeability entries, $\mu = \mu_o\mu_r$, where μ_r is relative permeability. The 4-transverse-field-component formulation in (7), can be simplified to

$$\begin{aligned}\int_s \Big[& E_t^* \cdot \omega\varepsilon_{tt} \cdot E_t + H_t^* \cdot \omega\mu \cdot H_t - \frac{1}{\omega\mu}\left[\nabla_t \times E_t\right]^* \cdot \left[\nabla_t \times E_t\right] \\ & - \frac{1}{\omega\varepsilon_{zz}}\left[\nabla_t \times H_t - j\omega\varepsilon_{zt} \cdot E_t\right]^* \left[\nabla_t \times H_t - j\omega\varepsilon_{zt} \cdot E_t\right]\Big] ds \\ & = \beta \int_s z \cdot \left[E_t^* \times H_t + E_t \times H_t^*\right] ds\end{aligned} \quad (8)$$

Also, the longitudinal field component E_z remains as shown in (5), but H_z simplifies to

$$H_z = \frac{-1}{j\omega\mu}\left[\nabla_t \times E_t\right] \quad (9)$$

This formulation solves for the propagation constant, β, and the modal field patterns when the geometry, material parameters and signal frequency are predefined. This E_t and H_t formulation has not previously been applied to gyroelectric structures.

III. Results And Analysis

The finite element model has been implemented successfully in FEMLAB®. A partially-filled dielectric loaded waveguide, a magnetised ferrite-loaded waveguide [4,6] and a semiconductor-loaded (using n-type, gallium arsenide, GaAs) waveguiding structure [5] have been used to validate the formulation. The theoretical and FEM results show good agreement. Nonreciprocal behaviour is observed for gyrotropic structures.

The insert in Fig. 1 illustrates a two-layer air-semiconductor waveguiding structure between two perfectly conducting planes. The air region has a thickness of P_1 = 80μm, and the semiconductor layer thickness P_2 = 100μm. It is assumed that there is no field variation in the y-direction, $\partial/\partial y = 0$ (it is modelled with magnetic walls in the FEM implementation). The analysis is limited to transverse magnetic (TM) wave modes only, i.e. E_x, E_z and H_y field components. A closed form solution has been derived by Mohsenian et al [5] and has been used to provide comparison with the 4-transverse field component formulation. We have verified Mohsenian's results with n-type GaAs and these are not repeated here. However, Fig. 1 has been computed using parameters corresponding to intrinsic indium antimonide, InSb, at 300K with a relative permittivity constant of 17.7, and a carrier concentration, $N_e = 1.1\times10^{22}m^{-3}$. This material is more suitable for terahertz frequencies. The permeability is assumed to be a constant for both regions. A static magnetic field, $\mathbf{B_o}$ of 0.98 Tesla is applied in the direction parallel to the interface, i.e. y-direction. The semiconductor medium becomes an asymmetrical tensor, which takes the form of

$$[\varepsilon] = \varepsilon_o \begin{bmatrix} \xi & 0 & -j\eta \\ 0 & \zeta & 0 \\ j\eta & 0 & \xi \end{bmatrix} \quad (10)$$

where the tensor elements are defined in [1,2,3]. It can be seen that excellent agreement exists between the data for the forward and reverse solutions computed from the exact dispersion relation and the finite element result. Nonreciprocal effects are evident between the forward and the reverse propagation constants. The differential phase constant increases as the frequency increases.

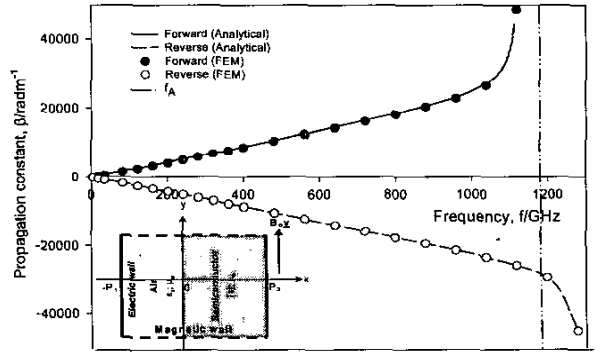

Fig. 1: Dispersion characteristics of a pair of parallel plates with air-InSb fillings [ε_r = 17.7, B_o = 0.98 Tesla, $N_e = 1.1\text{x}10^{22}$ m^{-1}, f_A = 1173.6GHz]

Another gyroelectric structure to be presented in this paper is a partially loaded rectangular waveguide with a semiconductor slab. A dc magnetic field is applied to the semiconductor in the direction parallel to the interface as depicted in Fig. 2. A few investigators have discussed the structures either partially or totally filled with a magneto-semiconductor, sometimes transversely magnetised [7-9]. However, material characterisation and full-wave analysis is still at an early stage and more extensive research, such as that outlined in this paper, is required to develop nonreciprocal control components for sub-millimetre and millimetre wavelengths.

The partially semiconductor loaded waveguide in Fig. 2 has dimensions of a = 300μm, b = 200μm, h = 50μm. Similarly to the parallel plate case, the semiconductor modelled here is lossless InSb operating at 300K. The region above the semiconductor slab is air.

The nonreciprocal behaviour of the magneto-semiconductor partially loaded waveguide is illustrated in Fig. 3 where the propagation constants for forward and reverse propagation are not equivalent. This results in a phase constant split. The mode with the lowest cut-off frequency is known as the dominant mode and is indicated in Fig. 3. It may be observed that the cut-off frequency is approximately 500GHz. From hollow waveguide theory, the dominant mode is the TE^z_{10} mode that has a cut-off wavelength given by, $\lambda_c = 2a$. An approximation of the cut-off wavelength is therefore $\lambda_c = 600\mu m$ and the cut-off frequency is hence approximated to be $f_c = 500GHz$. But, from the curve, the cut-off frequency is not exactly at 500GHz due to the fact that the waveguide is an inhomogeneously filled medium. In other words, the cut-off frequency is lower than 500GHz because the effective permittivity is slightly higher than ε_o.

As the frequency increases, the differential phase shift, $\Delta\beta = \beta^+ - \beta^-$, increases for the dominant mode as illustrated in Fig. 4. The relative effective permittivity (ε_{eff}) of the semiconductor, which is a function of frequency and bias field, is defined as [1,2]

$$\varepsilon_{eff} = \frac{\xi^2 - \eta^2}{\xi} \tag{11}$$

At frequency f_A, $\varepsilon_{eff} = 0$; below f_A, $\varepsilon_{eff} < 0$ and above f_A, $\varepsilon_{eff} > 0$. When $\varepsilon_{eff} > 0$, the field concentrates inside the semiconductor as shown in Fig. 7. When $\varepsilon_{eff} < 0$, the field resides principally in the air as shown in Figs. 5 and 6. Fig. 6 corresponds to a frequency with split phase constants and this is reflected in the different field patterns for forward and reverse propagation.

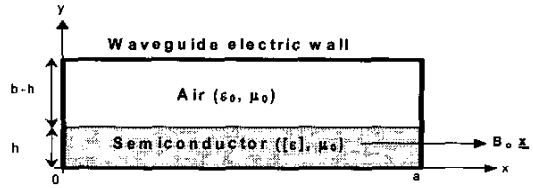

Fig. 2: A partially loaded hollow rectangular waveguide with gyroelectric semiconductor.

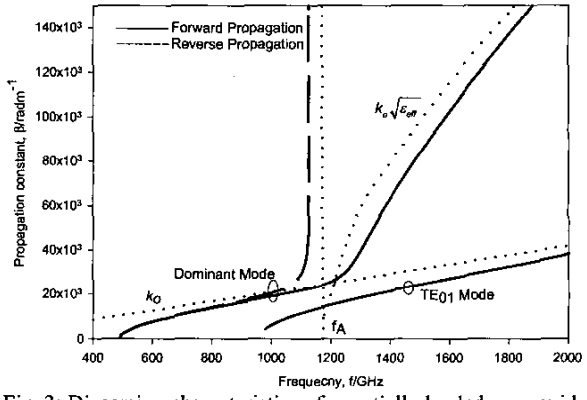

Fig. 3: Dispersion characteristics of a partially loaded waveguide with magnetised semiconductor. [$\varepsilon_r = 17.7$, $B_0 = 0.98$ Tesla, $N_e = 1.1\times10^{22}$ m^{-1}, $f_A = 1173.6$GHz]

Fig. 3 also depicts the dispersion characteristic of a quasi-TE_{01} mode. The cut-off frequency can be approximated from the hollow waveguide theory in which a TE^z_{01} mode in a waveguide of size $a\times b$, where $a > b$, has a cut-off wavelength given by $\lambda_c = 2b$, where b is the height of the hollow waveguide. The cut-off frequency is hence approximated to be $f_c = 1000GHz$, which agrees well with Fig.3.

From the TE_{01} mode dispersion characteristic curves, the splitting of the phase constants is negligible. In other words, the nonreciprocal behaviour is not apparent in this TE_{01} mode. With reference to Fig. 8, this can be explained from the $\boldsymbol{E}_t$ distribution, where the arrow plot shows the E_x field component dominates. As a result, the interaction between the static magnetic field, $\mathbf{B}_0$, and the transverse electric $\boldsymbol{E}_t$, is a minimum since the E_x field component is parallel to $\mathbf{B}_0$. The gyroelectric behaviour of the semiconductor is not achieved and no significant non-reciprocal behaviour occurs for this TE_{01} mode. As frequency increases, the propagation constant increases asymptotically towards the plane wave phase constant of the air region, $k_0 = \omega\sqrt{\varepsilon_0\mu_0}$. It is noteworthy that the field is almost excluded from the InSb slab and this is due to the fact the relative permittivity term appropriate for this orientation is ζ and its value is –25.95.

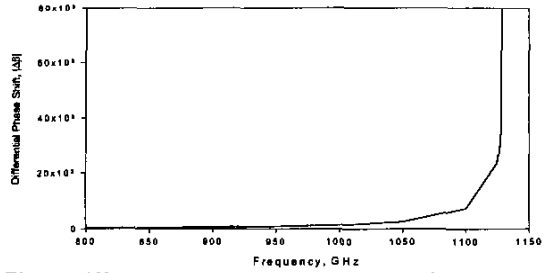

Fig. 4: Differential phase shift of dominant mode.

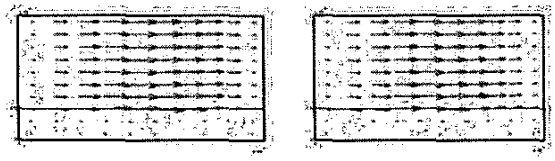
(a) Forward Propagation (b) Reverse Propagation

Fig. 5: Dominant mode $\mathbf{H}_t$ field components distribution across the waveguide in Fig. 2 at 600GHz.

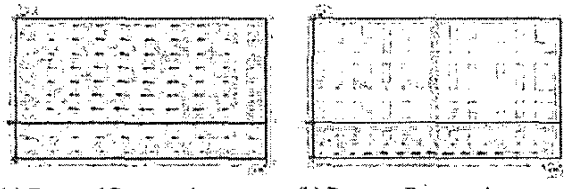
(a) Forward Propagation (b) Reverse Propagation

Fig. 6: Dominant mode $\mathbf{H}_t$ field components distribution across the waveguide in Fig. 2 at 1129GHz

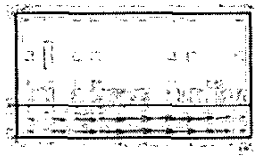

Fig.7: Dominant forward propagation mode $\mathbf{H}_t$ field components distribution across the waveguide in Fig. 2 at 1500GHz

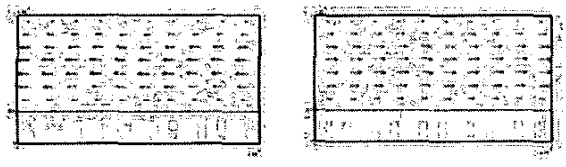
(a) Forward Propagation (b) Reverse Propagation

Fig. 8: TE_{01} Mode $\mathbf{E}_t$ field components distribution across the waveguide in Fig.2 at 1250GHz.

In summary, the nonreciprocal behaviour of the semiconductor loaded rectangular waveguide has been modelled and evaluated for the dominant mode quasi-TE_{10}. However, as expected, nonreciprocal behaviour does not occur with the TE_{01} mode, which has the transverse electric field parallel to the applied static magnetic field

IV. Conclusion

The novel general solver for gyrotropic structures described in this paper has been shown to be very versatile in its applicability to a variety of structures. One potential nonreciprocal gyroelectric phase shifter structure has been reported and the solver will be used to explore other inhomogeneous gyroelectric waveguides for terahertz frequencies.

Acknowledgement

The authors wish to acknowledge the assistance and support of FEMLAB®.

References

[1] C. K. Yong, R. Sloan and L.E. Davis, "A Ka-band indium antimonide junction circulator," *IEEE Trans. Microwave Theory Tech.*, vol. MTT-49, no.6, pp.1101-1106, Jun. 2001.

[2] R. Sloan, C. K. Yong and L. E. Davis, "Broadband theoretical gyroelectric junction circulator tracking behavior at 77K," *IEEE Trans. Microwave Theory Tech.*, vol. MTT-44, no. 12, pp. 2655-2659, Dec. 1996.

[3] D. M. Bolle and S. H. Talisa, "Fundamental considerations in millimetre and near millimetre component design employing magnetoplasmons," *IEEE Trans. Microwave Theory Tech.*, vol. MTT-29, pp. 61-72, Sept. 1981.

[4] T. Angkaew, M. Matsuhara, and N. Kumagai, "Finite-element analysis of waveguide modes: A novel approach that eliminates spurious modes," *IEEE Trans Microwave Theory Tech.*, vol. MTT-35, no.2, pp. 117-123, Feb. 1983.

[5] N. Mohsenian, T. J. Delph, and D. M. Bolle, "Analysis of waveguiding structures employing surface magnetoplasmons by the FEM," *IEEE Trans. Microwave Theory Tech.*, vol. MTT-35, no. 4, pp. 464-468, April 1987.

[6] L. Zhou and L. E. Davis, "Finite-element method with edge elements for waveguides loaded with ferrite magnetised in arbitrary direction," *IEEE Trans. Microwave Theory Tech*, vol. MTT-44, no. 6, pp. 809-815, June 1996.

[7] Roberto Sorrentino, "Exact Analysis of Rectangular Waveguides Inhomogeneously Filled with a Transversely Magnetized Semiconductor," *IEEE Trans. Microwave Theory Tech.*, vol. 24, no. 4, pp. 201-208, April 1976.

[8] Richard M. Arnold, and F. J. Rosenbaum, "Nonreciprocal wave propagation in semiconductor loaded waveguides in the presence of a transverse magnetic field," *IEEE Trans. Microwave Theory Tech.*, vol.19, no.1, pp.57-65, Jan. 1971.

[9] R. Hirota, and K. Suzuki, "Field distribution in a magnetoplasma-loaded waveguide at room temperature," *IEEE Trans. Microwave Theory Tech.*, vol. 18, no.4, pp. 188-195, April 1970.